Sustainable Energy & Fuels

ROYAL SOCIETY OF CHEMISTRY

PAPER

View Article Online
View Journal | View Issue

Check for updates

Cite this: *Sustainable Energy Fuels*, 2024, **8**, 546

Measuring metal halide perovskite single cell degradation consistent with module-based conditions†

Robert Tirawat, *[a] Amy E. Louks,[bd] Mengjin Yang,[b] Severin N. Habisreutinger,[a] Jao van de Lagemaat,[ac] Soňa Uličná,[a] Ross A. Kerner,[a] Kai Zhu,[a] Laura T. Schelhas,[a] Axel F. Palmstrom[b] and Joseph J. Berry*[bc]

In past years, there has been progress towards increasing the efficiency of metal halide perovskite solar cells (PSCs) without sacrificing long-term stability. However, preventing or mitigating degradation remains one of the major challenges for the commercialization of PSCs. Researchers must ensure that information learned from cell-level studies is relevant to the ultimate target of module application. In this work, we demonstrate that the bias condition used during aging studies has a measurable impact on degradation. We compared the performance of a large number of devices (n = 486) which were aged either under open-circuit (OC) or quasi-maximum power point (qMPP) conditions. The performance losses between the two conditions are found to be correlated, but notably, aging at OC leads to a more rapid performance decrease. Furthermore, this faster degradation in the OC condition compared with the qMPP condition occurs regardless of device stack design, treatments, or additives as demonstrated across approximately 160 variants of the p-i-n device stack. The OC condition is an important factor for field stability because partial shading of a module can result in individual cells going into OC. The fact that the degradation dynamics between qMPP and OC conditions are highly correlated indicates that aging studies at OC are related to relevant degradation processes. Consequently, stability studies to generate relevant insights into the degradation processes of PSCs can be executed without requiring sophisticated electronic infrastructure. However, care must be taken with cell-level experimental configurations because unintended, artificial degradation mechanisms may arise that are either not relevant to the application (*e.g.*, modules) or obfuscate the results of the study being undertaken.

Received 29th September 2023
Accepted 27th December 2023

DOI: 10.1039/d3se01268a

rsc.li/sustainable-energy

1 Introduction

Metal halide perovskites (MHPs) are a promising material for widespread implementation of photovoltaics (PVs). Perovskite solar cells (PSCs) have the advantage of high-power conversion efficiencies (PCE), exceeding 26%,[1] while being cost-effective and having many avenues for fabrication. However, for PSCs to be a commercially viable technology, performance must be understood and established. In this case, high performance refers to maintaining a high PCE coupled with long term stability (PCE over time). Conventional, well-established PV technologies such as c-Si and CdTe have proven to be able to operate for many decades with only marginal performance losses. This achievement is the result of a multi-decade research and development effort. Perovskite PV, having emerged merely a decade ago, is now facing the challenge of compressing decades of research into a few years to match the long-term performance of the current technologies.

A major step forward was the establishment of standard protocols for testing long-term performance as outlined by the International Summit on Organic Photovoltaic Stability (ISOS) consensus statement.[2] Here, specific sets of parameters and conditions are detailed for running stability studies of PSCs with a variety of stressors. It is important to highlight that these protocols have largely emerged from conceptual considerations and previous learning from other fields, but still need to be validated by operational outdoor studies – specifically how ISOS protocol results map onto performance in the field. Nevertheless, generally aligning laboratories on similar stressing protocols is a vital step towards harmonized approaches for improving long-term performance.

[a]*Chemistry and Nanoscience Center, National Renewable Energy Laboratory, Golden, Colorado 80401, USA. E-mail: Robert.Tirawat@nrel.gov*

[b]*Materials Science Center, National Renewable Energy Laboratory, Golden, Colorado 80401, USA. E-mail: Joe.Berry@nrel.gov*

[c]*Department of Physics, Renewable and Sustainable Energy Institute, University of Colorado, Boulder, Colorado 80309, USA*

[d]*Department of Chemistry, Colorado School of Mines, Golden, CO, 80401, USA*

† Electronic supplementary information (ESI) available. See DOI: https://doi.org/10.1039/d3se01268a

Important major stressing parameters outlined in the protocols as proxies for stressing under operational conditions include light, elevated temperature, and moisture. The importance of light and elevated temperature to predicting outdoor stability has been recently demonstrated;[3] however, specifically for MHP based solar cells, another critical parameter is the electrical load. MHP absorbers are unique compared with other semiconductors in that they exhibit a strong ionic response to external bias. One prominent way this behavior has been observed is in the current–voltage hysteresis, where the scan direction of the voltage sweep will impact the extracted photocurrent. This has largely been attributed to constituent ions responding to the changing external bias and consequently modifying the energetics of the interfaces.[4] Furthermore, electrochemical pathways, with their link to the defect structure of the MHP active layers, have been identified as critical degradation mechanisms that must be understood in the context of PV performance to further enhance the long-term stability of PSCs. In fact, it was recently demonstrated that voltages near the maximum power point (V_{MPP}) or open-circuit voltage (V_{OC}) can drive electrochemical reactions involving defect and lattice halide species in PSCs.[5,6] Thus, depending on MHP composition and device design, the presence of bias may accelerate certain electrochemical or photoelectrochemical degradation processes and affect the long term stability.[7,8] For long-term performance studies of PSCs, it is therefore very likely that the external load will have a significant impact.

For operational stability studies under simulated solar illumination, ISOS protocols specify either maximum power point (MPP) or open-circuit (OC) load for the basic and intermediate levels but restrict the load to MPP for the advanced level. The third, most advanced level of ISOS protocols requires active tracking of the maximum power point (MPPT). The lower-level protocols allow for the MPP condition to be met by holding the bias near V_{MPP}, as determined from an initial current–voltage sweep. A common approach is to use a static load resistor to hold devices near V_{MPP}, which will be referred to as quasi-MPP (qMPP) in this work.

A brief literature review of recent papers show that research groups are generally following the ISOS guidelines, though detailed reporting of aging protocols followed remains inconsistent.[9–18] Of the studies reviewed, half were done at MPP, some studies were performed at OC, while many of the studies did not specify the load conditions. Additionally, there is a lack of aggregated stability data across PSC designs which would be useful to identify degradation pathways that may not be readily apparent from individual and isolated studies. These challenges aside, demonstrations of stability have increased in duration,[19] making examinations of specific mechanisms a priority to rationally improve PSC performance.

Here, we provide a comparative study across multiple device designs (*i.e.*, the specific layers within the p-i-n stack) and multiple MHP compositions in which the operational stress has been set to OC or MPP conditions for nominally identical devices. This change in static test conditions represents two distinct sets of stresses within the device which will modulate both the current through the device and the electric fields within the stack. We demonstrate the role that bias conditions play in how PSCs degrade across a large and varied sample set, permitting insight into different operational stresses. We observe that there is a distinct difference in the degradation rate for devices held at OC compared to devices held at qMPP. Crucially, we find that OC conditions lead to a more severe performance decline. Moreover, we find that laboratory-scale single cell devices, which differ significantly in their layout from a module, display degradation modes that are specific to both the substrate layout as well as masked *versus* unmasked illumination conditions. We show that this is a direct result of photo-induced bias within and around the active area of the device. Our results suggest that the device layout may activate unique degradation pathways which have a significant negative impact on the long-term device performance. In fact, this may lead to an underestimation of the operational stability, as those degradation modes may not be present in cells incorporated in modules. We conclude by providing recommendations for single cell device fabrication and testing conditions that will minimize such measurement artifacts by evaluating single cell stability in a way that approximates conditions likely to be found in a full module.

Following our guidance, researchers can be more confident that the observed performance decline in stability studies on research PSCs is caused by relevant degradation processes rather than by laboratory measurement artifacts. Tackling those mechanisms has then the potential to directly translate into longer operational lifetime of deployed modules. Overall, our work leads to the conclusion that mechanistic insight into degradation of MHP single cells is critical and failure to consider known mechanisms in cell layouts can often lead to premature cell failure.

2 Experimental

We have examined a wide range of device designs common for PSCs with a p-i-n architecture. In this work, we focused on studies using lead-halide perovskites of the form of $APb(I_x-Br_{1-x})_3$ where the A-site cation were various combinations of methylammonium (MA, $CH_3NH_3^+$), formamidinium (FA, $CH_3(NH_2)_2^+$), and Cs. Different ratios of iodine to bromine were also examined. In addition to variations in the active layer, we explored many different device stacks (*e.g.*, electron transport layers (ETLs), hole transport layers (HTLs), electrodes) and treatments (*e.g.*, additives, post-treatments). After the devices were aged, the data of approximately 160 variations of the p-i-n stack, shown in Fig. 1a, comprising 486 individual substrates were aggregated and examined. A subset of the best performing variations of this set was reported in more detail by Louks *et al.*[20] The materials and treatments used in this work are summarized in Table S1.†

The stability of these samples was evaluated in our Stability Parameter Analyzer (SPA) system in a modified ISOS-L-2I test.[21] Samples were loaded into a flow cell with an inert (N_2) atmosphere, illuminated at 0.77 suns, and held at elevated temperature (55 °C or 70 °C). The PSCs were periodically characterized by a current–voltage (*J–V*) sweep. Between *J–V* sweeps, devices

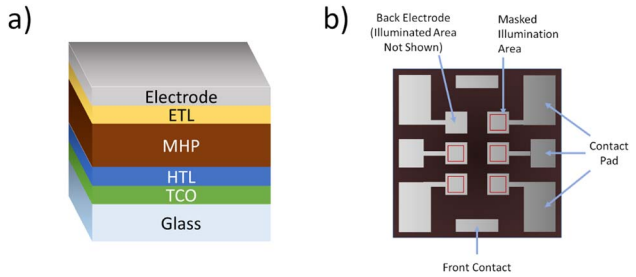

Fig. 1 (a) Architecture of p-i-n perovskite device stack. (b) Metallization patterning of PCSs. Active area is defined by the square electrode pad. Red squares indicate illumination area defined by shadow mask.

were connected to a load resistor to hold them in a qMPP condition. Each sample (*i.e.*, substrate) was patterned with six PSC devices, which will henceforth be referred to as pixels, as shown in Fig. 1b. For these samples, two pixels were under active test as described above, and four pixels were held in an OC condition and not *J–V* swept during aging. Samples were aged for one week, then removed from the SPA and characterized with a solar simulator. The primary purpose of samples referenced in this work was the development of scalable deposition techniques and the evaluation of operational performance as defined above. The approach used was to rapidly iterate device designs with the aim of improving short-term and long-term PV performance. Both are critical towards transitioning this PV technology from the lab to the field. To that end, temperatures and aging duration were selected to induce a measurable, but not catastrophic, change in PCE for timely feedback to evaluate the effectiveness of the device strategies being implemented. While samples were aged both with and without masks, the short aging duration was insufficient for illumination outside of the active area to stimulate the degradation mechanism discussed in Section 3.3 and impact stability results.

In addition to the rapid one-week stability study discussed above, we conducted a long-term, ISOS-L-2I stability study to determine the effect of masking substrates during aging (Section 3.3). Samples were aged in our SPA system at 1 sun illumination at 65 °C in a nitrogen atmosphere. One set of samples were fully illuminated, and a second set used shadow masks to restrict illumination to 0.06 cm^2 within the larger 0.122 cm^2 active area as defined by the back electrode (Fig. 1b).

3 Results & discussion

3.1 OC aging is harsher than qMPP aging

Many cells in a module may experience an OC condition for extended periods of time while in field service. Typical modules contain strings of cells connected in series; when one of these cells is shaded, the other cells in the string are held at V_{OC}. Thus, the partial shading stability issue is not only a reverse bias stability challenge, but also a forward bias/V_{OC} stability challenge. Our results suggest that cells should be evaluated at both V_{MPP} as well as V_{OC} to understand module-level operational stability under ideal and non-ideal implementation. These measurements also provide insight on some of the primary stresses that are seen in cells and would be anticipated to manifest in module performance over time.

Previous studies have shown that OC conditions may lead to more rapid degradation. It has been suggested that OC aging may result in degradation arising from formation of deep-trap states, phase segregation, charge accumulation, and increased ion migration.[22–25] However, these studies have largely focused on the effects on a few, specific PSC active layers or architectures. Here we demonstrate through analysis of a data set spanning a large number of PSC devices and variations of this device stack that the increased degradation observed from OC aging is more generally applicable to PSCs, at least for the p-i-n architecture.

We begin by presenting statistics ($n = 486$) on the effect of accelerated aging of devices in a qMPP condition *versus* those in an OC condition. To examine the differences of the post-aging PCE across the qMPP and OC conditions, we plot the average PCE, measured *ex situ* in a solar simulator, for pixels aged in the OC and qMPP bias conditions as shown in Fig. 2. Each point in the figure represents a single substrate with the mean PCE of pixels on a substrate after stressing under OC conditions plotted against the mean PCE of pixels on the same substrate that were stressed at qMPP conditions. Initial device data of the cells to be stressed under the different conditions are shown in black. Outlier samples with poor yield (*i.e.*, where initial $PCE_{OC} \neq PCE_{qMPP}$ within the interquartile range) were excluded; however, exclusion of these outliers does not impact the

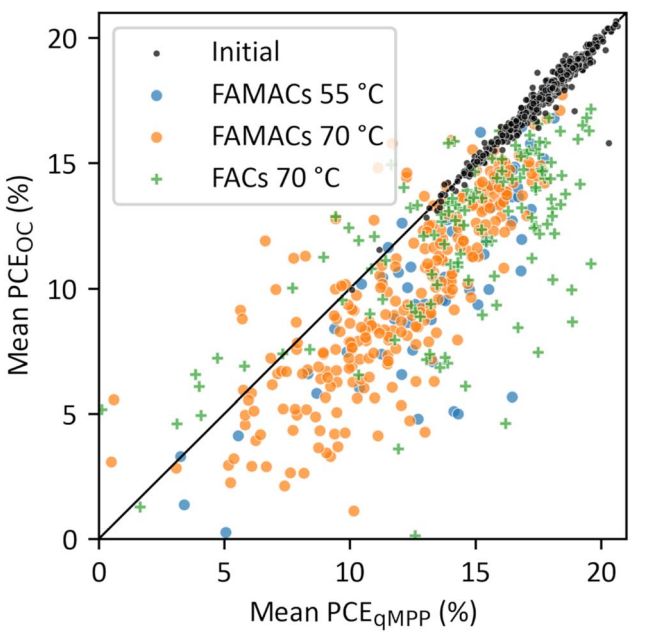

Fig. 2 Mean PCE of devices aged in an OC condition plotted against mean PCE of devices aged in a qMPP condition on the same substrate. Initial data are shown in black while post-aging data are shown in blue, orange, and green. A one-to-one parity line is shown for reference. Data is shown for triple-cation (FAMACs) and double-cation (FACs) PSCs with various device layers, additives, and treatments (Table S1†). Samples were aged for 168 h under illumination at 55 °C or 70 °C.

conclusions presented here (Fig. S2†). Plots for the other optoelectronic properties and individual groupings are shown in Fig. S3.† The initial device data indicates that the devices have a high initial PCE and low spread, as may be observed by data proximity to the parity line where $PCE_{OC} = PCE_{qMPP}$.

The OC efficiencies are correlated (Pearson correlation coefficient = 0.78) with the qMPP efficiencies following aging. As Fig. 2 shows, the data mostly lie below and to the right of the parity line, meaning pixels aged in an OC condition demonstrate lower PCE after aging than their sister pixels aged in a qMPP condition on the same sample. This trend holds true for triple-cation (FAMACs) and double-cation (FACs) MHP active layers with varying halide ratios, for the approximately 160 variations in treatments, additives, and architectures used (not differentiated in the figure), and for aging at 55 °C and 70 °C. This result confirms that OC is a harsher condition than qMPP for most stability studies, regardless of PSC design, and shows the relevance of OC aging studies. An OC stability study requires little more than a light source and a hot plate, in comparison to a qMPP or MPPT system which requires sophisticated electronics. Based on the correlation between the two conditions shown here, insights and hypothesis testing of stability mechanisms may be gained from the more facile approach of an OC aging study.

3.2 OC perovskite degradation

Regional potential differences in PSCs have been identified as a pathway to induce degradation in PSCs.[26–31] Potential differences out-of-plane can result in the release of iodine species[26,27] while in-plane potential differences may result in migration of ions.[28] Both mechanisms can lead to the degradation of pixel electrodes as the metal contact reacts with released halides. Under illumination of uncontacted MHP absorber material outside of the active area, a bias is generated across the active area that is near V_{OC}, as shown with modeling in Fig. 3a and b.

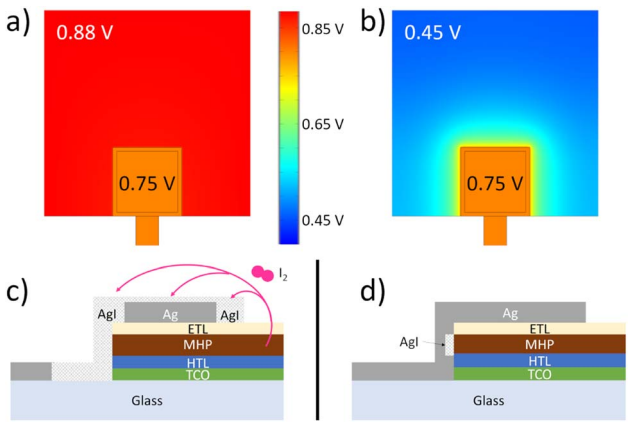

Fig. 3 Modeling of bias across the active layer of an (a) unmasked and (b) masked device under illumination. The electrode is outlined with the inset square representing the apertured area. Mechanisms affecting degradation rate and dropout for (c) unmasked and (d) masked devices.

In short, the device layout was modeled with the active layer represented by a simple diode system generating photocurrent between the ITO electrode and the top C_{60}/BCP/silver electrode. Fig. 3a and b show simulated devices held at approximately MPP conditions (V_{MPP} = 0.75 V). Light shading of the system was modeled by only generating photocurrent in an area slightly smaller than the silver contact pad. Lateral current transport towards the silver pad electrode is possible in the top layer through (inefficient) conduction in the C_{60} and BCP layers. It is clear from the simulated potential that in the case of full illumination, the area outside of the silver electrode becomes biased around open circuit conditions (0.88 V for the simulated parameters), while for the shaded device, the potential on the top of the layer stack decays away from the top-silver electrode pad.

The large, photo-induced bias of MHP outside of the active area may result in release of iodine from the MHP layer.[26] Additionally, lateral migration of negative ions into the active area may be promoted by the higher potential of the MHP surrounding the active area.[28] Both mechanisms contribute to the degradation of the Ag electrode from the edge in and top down (Fig. 3c). This effect may be mitigated with shadow masks which prevent illumination of the MHP absorber outside of the active area. Halide diffusion through the ETL in the active area does not appear to be a significant contributor to electrode degradation as discussed in the following section.

In the masked instance, without passivation or barrier layers between the MHP and metal electrode, degradation is limited to the area where metal is in direct contact with the MHP (Fig. 3d). When performing stability studies on individual cells, the masked configuration exhibits degradation modes more representative to what might occur in a module where the majority of the device area will be covered by metal electrodes and buffer layers.

3.3 Validation of the OC degradation mechanism

We have experimentally observed the impact that bias has on the degradation of PSCs. Replicate $FA_{0.87}MA_{0.08}Cs_{0.05}Pb(I_{0.92}Br_{0.08})_3$ PSCs were fabricated in the p-i-n structure as described in the Experimental Methods section (see ESI†). The PSCs were constructed on indium-doped tin oxide (ITO) coated glass with a NiO_x/poly(triaryl amine) (PTAA) bilayer as the selective HTL, C_{60}/bathocuproine (BCP) as the selective ETL, and a silver electrode as a low-resistance metal contact (Fig. 4a). The optoelectronic properties of the finished devices were characterized with a solar simulator (Fig. 4b). Following the initial characterization, samples were loaded into the SPA system for aging. In the SPA system, half of the pixels were fully illuminated while the other half were covered with a shadow mask to aperture the illuminated area down to 0.06 cm^2 (Fig. 1b). We aged the samples in the SPA system under 1 sun irradiance at 65 °C in a nitrogen atmosphere. Pixels were held at qMPP and characterized with *J–V* sweeps with an interval of approximately 75 min.

The masked samples maintained 90% of their initial performance, even after 1000 hours. The unmasked samples, in

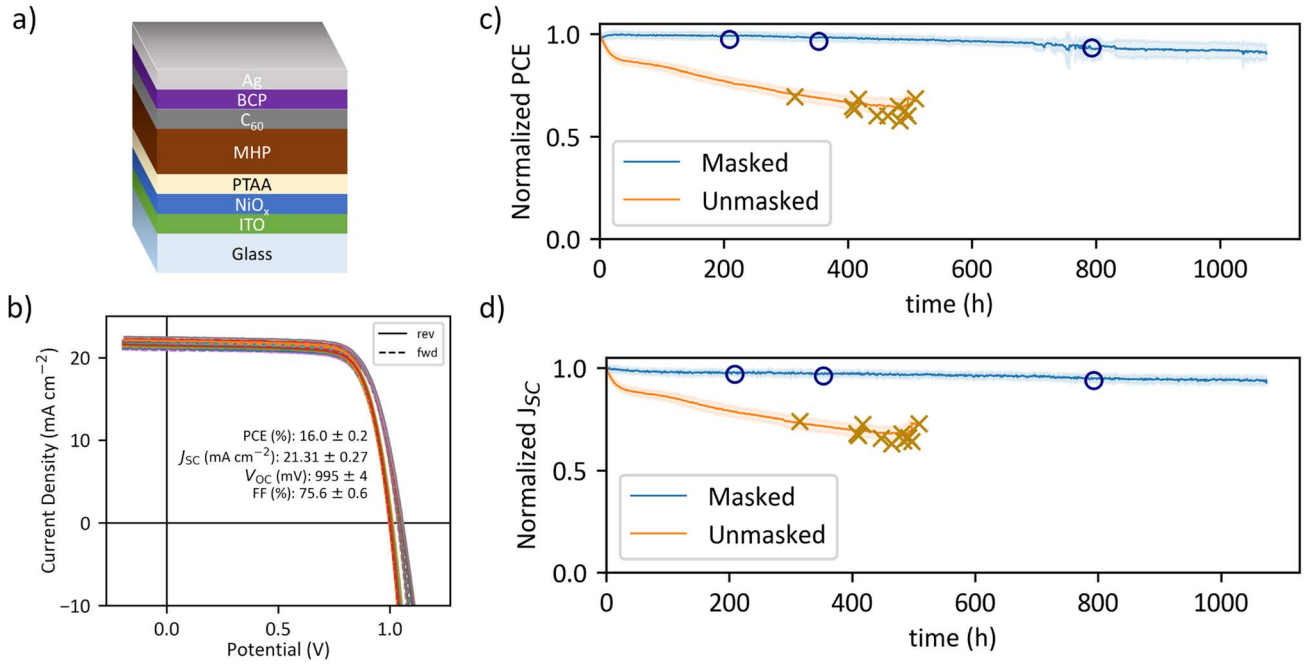

Fig. 4 (a) Device architecture used in masking study. (b) Initial performance of masking study devices as measured on a solar simulator before aging. Normalized PCE (c) and J_{SC} (d) of devices during aging. X and O markers in the plots indicate the time and final figure of merit value of devices before device dropout or step-edge failure, respectively.

stark contrast, had dropped down to below 90% of initial performance within the first 30 hours. Afterwards, they appear to transition to a slower, linear degradation rate. The faster degradation rate in the PCE of the unmasked samples compared to the masked samples can largely be attributed to a corresponding drop in short-circuit current density (J_{SC}) (Fig. 4c and d). V_{OC} and fill factor (FF) remain largely unchanged for both unmasked and masked samples (Fig. S4†). By 500 hours, the average performance of the unmasked samples had dropped to 65%.

After approximately 300 hours, we began to observe sudden and catastrophic pixel failure in the unmasked sample set, where the pixels would suddenly be measured as an open circuit (Fig. S5a†). We call this behavior pixel "dropout" and is indicated by the Xs in Fig. 4c and d. By 510 hours, every single unmasked pixel failed in this manner. A few of the masked samples did fail in aging; however the degradation behavior was markedly different. The masked samples did not exhibit any loss in optoelectronic properties prior to failure. Instead, the masked samples began to have anomalous measurement behavior where the *J–V* curves became very noisy and discontinuous resulting in large fluctuations in the optoelectronic properties (Fig. S5b†). This different degradation mechanism is marked with Os in Fig. 4c and d.

Once the unmasked samples were removed from the test setup, we could observe significant corrosion of the electrodes (Fig. 5a). In contrast, no visual corrosion was observed for the masked sample electrodes (Fig. 5b). The unmasked electrode corrosion appeared to be growing from the electrode edges toward the center of the electrode and resulted in a color change and roughening of the metal electrode. Corrosion of the active area was not total; however, the narrow metallization traces connecting the electrode to the external contact pad appeared wholly compromised. The failure of these traces resulted in electrical disconnection, explaining the sudden failure of these pixels observed during aging. In fact, by redepositing the metal electrode on top of the corroded electrodes of an unmasked pixel after it had failed *via* pixel dropout, we were able to re-establish functionality in the pixel, thus confirming corrosion-induced breakdown of the metal traces as the cause of sudden dropout failure (Fig. 5c). This indicates that, alongside the visible corrosion of the electrode, the metal traces became non-conductive. The fast initial degradation rate of the unmasked pixels could be explained by corrosion of the metal electrodes from the edge in, effectively reducing the active area of the pixel where charge carriers can be collected which in turn accounts for the observed decrease in photocurrent.

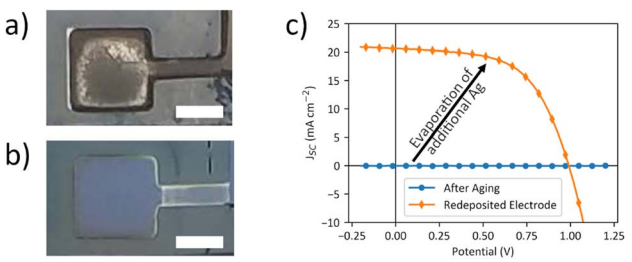

Fig. 5 Post-aging photographs of an (a) unmasked and (b) masked pixels with 2 mm scale bars. (c) Recovery of a dropout pixel performance after depositing additional Ag on top of the old electrode.

To elucidate the process underlying the observed corrosion, we performed post-aging X-ray photoelectron spectroscopy (XPS) which shows the presence of iodine at the surface of the metal electrode of unmasked samples. While iodine is also present at the metal electrode surface of the masked pixel, elemental quantification of the survey scan (Fig. 6a) confirms a substantially lower I/Ag ratio in this pixel as shown in Table 1. Further, high resolution XPS scans (Fig. 6b and c) at the delaminated perovskite/metal electrode interface detected no Ag and measured negligible I signals in the masked sample, whereas there is significant presence of both Ag and I in the unmasked sample. The lack of Ag and I signal at the perovskite/metal interface makes it less likely that interfacial diffusion is the primary pathway for electrode degradation and places the source of the iodine outside of the active area. Analysis of the XPS Ag 3d and I 3d peak positions confirms the formation of AgI in the unmasked pixel. The XPS data support the hypothesis that iodine escapes the MHP layer in form of volatile I_2 and subsequently reacts with the Ag electrode from the top, as shown in the mechanism schematic in Fig. 3, instead of diffusing into the electrode through the interfaces. These observations are in line with previous reports describing degradation of silver electrodes through reaction with iodine to form AgI.[32,33] Presence of small amounts of iodine on top of the electrode of the masked pixel may be explained by cross-contamination between masked and unmasked samples within the shared flow cell used during stability studies; iodine release when the pixels are exposed to ambient light without masks when being transferred between characterization setups; or possibly by sample handling.

In the case of masked illumination, we expect insufficient release of I_2 vapor to fully corrode the Ag contacts, yet some pixels were observed to fail with an anomalous failure mode (Fig. 4c and d). As is common practice, we remove the thin film layers on the substrate periphery by scraping with a razor blade or laser ablation prior to metallization. This "edge-deletion" is often done to expose the front contact for metallization and to eliminate potential issues that might arise from "poke-through" of pogo pins at the contact pad. We attribute the pixel failure in the masked illumination aging studies to direct MHP/Ag interfaces (Fig. 3d) that enable premature device failure by corrosion. We have also observed that this step-edge interface may drastically reduce shelf life, even without illumination. Importantly, this step-edge and direct MHP/Ag interface are the same as those that can be created at the P2 scribe of a module (Fig. 7). Therefore, cell-level studies that employ edge-deletion naturally incorporate a P2 scribe failure mode into the experiment, and the combination of edge-deletion and masked illumination isolate a degradation mechanism relevant to full modules and real-world operation. It is essential to address this failure mode in modules by various strategies such as adding a buffer or passivation layer prior to deposition of the metal electrode.[34]

Table 1 At% of Ag and I from the XPS survey scan at the surface of the metal electrode ("metal") and at the perovskite interface ("perovskite") exposed by delaminating the electrode

	At%			
	Masked		Unmasked	
	Ag 3d	I 3d	Ag 3d	I 3d
Metal	87.7	12.3	74.8	25.2
Perovskite	—	—	70.7	29.3

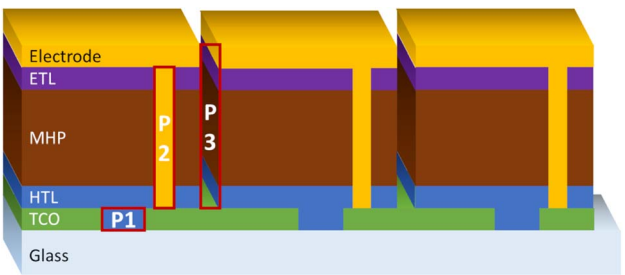

Fig. 7 Schematic of an interconnected module with P1, P2, P3, and P4 scribes indicated.

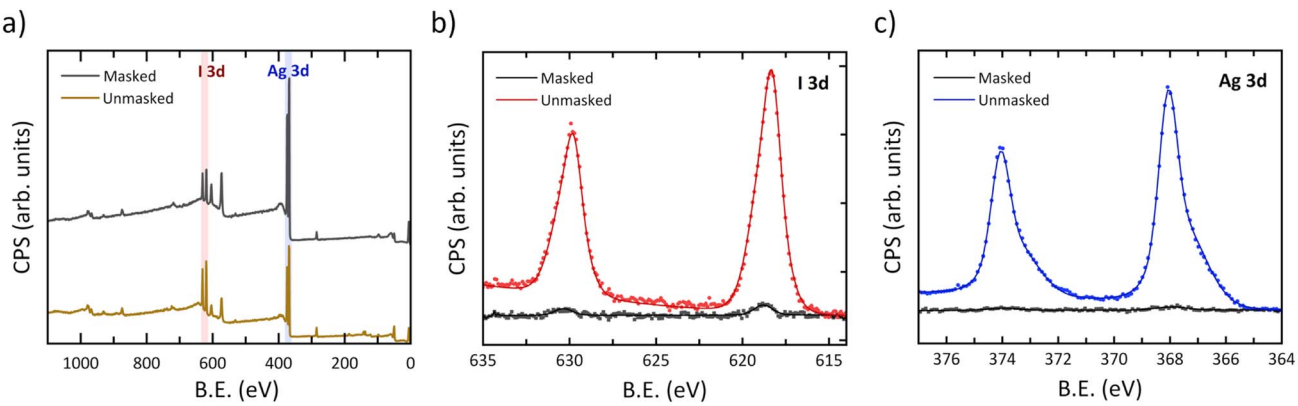

Fig. 6 (a) XPS survey scan from the metal covered pixel, (b) High resolution I 3d, and (c) Ag 3d XPS signals from perovskite/metal interface after delamination of the metal contact.

It is important to note that a module will have full coverage by metal or metal oxide electrodes inhibiting the release of volatile byproducts and will likely be encapsulated such that there is no head space for vapor transport. While this rapid degradation process caused by the device layout of research cells may not take place in full modules with the same kinetics, this is nevertheless a fundamental process that needs to be accounted for when designing cells and modules that are supposed to last for decades. By using shadow masks that limit the illumination to the active area of a cell during aging, this specific degradation pathway can be prevented, thus cutting off this module-irrelevant degradation artifact. Importantly, this will allow researchers to home in on more fundamental degradation processes which are likely to impair the long-term performance of PSCs when deployed in the field and, as a legitimate side effect, will result in an improvement of operational stability lifetime in the lab.

4 Conclusions

We have demonstrated that an OC condition increases the degradation rate of p-i-n PSCs during stability studies when compared to devices held in a qMPP condition. We find this to be true for devices with this architecture across a large variety of design variations including active layer composition, various additives, surface treatments, and device stacks. It is important to consider the stability of PSCs in the OC condition, as cells as parts of a module may experience periods at OC when other cells are shaded. Furthermore, this finding suggests that using light-soaking at OC conditions is a valid strategy for assessing and improving on the long-term stability of PSCs. In fact, we infer from our results that interventions which lead to increased stability under light-soaking at OC, should directly translate to significant improvements of operational lifetime in the field. Consequently, this relaxes the infrastructure requirements for academic and institutional labs for performing stability studies since all that is needed is a light source and a hotplate, dispensing with the need for complex, multi-channel electronics.

Furthermore, bias conditions across the entirety of the sample surface, not just those within the active area, may give rise to unintended effects during stability studies. Specifically, we have shown that without appropriate masking, the design of the device layout can lead to additional, artificial degradation for devices under constant illumination. We attribute this rapid degradation process to metal contact corrosion that effectively reduced the active area of the device, initially leading to a reduction in photocurrent and eventually to device failure. This effect was demonstrated for unmasked PSCs held at qMPP, and we expect that this pathway would be present and more pronounced for devices aged in an unmasked OC condition. We demonstrate that this specific degradation process dominates the performance decline of our devices. Consequently, it obfuscates other processes which may drive the degradation of PSCs in real-world applications such as modules and are therefore more relevant and generalizable. While illumination of the MHP area outside the active pixel area may not be relevant for modules, care must be taken when aging individual cells.

Based on these results, we recommend that cells are masked during aging whenever possible. Masking will serve to reduce additional degradation modes that are an artifact of the device design. Additionally, masking at cell-level studies can not only eliminate degradation specific to different cell layouts but is more directly related to the aging dynamics that PSCs would undergo in a module configuration. Care must also be taken with the details of device fabrication, particularly when removing the active layer, to expose the front contact for metallization or for other considerations, which may result in direct contact between the MHP absorber and metal contacts. A strategy aimed at preventing this mechanical failure mode can be to include the passivation and buffer layers developed for damage-free scribing in modules into individual device stacks.

Finally, our study highlights, once more, that MHPs exhibit unique electrochemical degradation processes which will require targeted research and development efforts on improved device layouts, halogen barriers, buffer layers, corrosion resistant contacts and similar strategies to enable multi-decadal performance with minimal losses when deployed at scale.

Author contributions

R. T., A. F. P., and J. J. B. conceived of the manuscript. R. T., A. E. L., M. Y., and S. N. H. fabricated and characterized perovskite solar cells under supervision of A. F. P. A. E. L. and R. T. conducted aging studies. R. T. curated data for this effort. J. v. d. L. conducted the physics model. S. U. conducted the XPS analysis under supervision of L. T. S. The original draft was written by R. T. under the supervision of J. J. B. with contributions from R. A. K. All authors reviewed the results and contributed to revision and editing of the manuscript.

Conflicts of interest

There are no conflicts to declare.

Acknowledgements

This work was supported by First Solar, Inc. under agreement CRD-13-00507-18 and by the U.S. Department of Energy Office of Energy Efficiency and Renewable Energy (EERE) under the Solar Energy Technologies Office (SETO) “Advanced Perovskite Solar Cells and Modules” program (Agreement Number 38256). X-ray photoelectron spectrsocopy for this work was supported in part by the Colorado Shared Instrumentation in Nanofabrication and Characterization (COSINC): the COSINC-CHR (Characterization) and/or CONSINC-FAB (Fabrication), College of Engineering & Applied Science, University of Colorado Boulder.

References

1 Best Research-Cell Efficiency Chart, https://www.nrel.gov/pv/cell-efficiency.html.

2 M. V. Khenkin, E. A. Katz, A. Abate, G. Bardizza, J. J. Berry, C. Brabec, F. Brunetti, V. Bulović, Q. Burlingame, A. Di Carlo, R. Cheacharoen, Y.-B. Cheng, A. Colsmann, S. Cros, K. Domanski, M. Dusza, C. J. Fell, S. R. Forrest, Y. Galagan, D. Di Girolamo, M. Grätzel, A. Hagfeldt, E. von Hauff, H. Hoppe, J. Kettle, H. Köbler, M. S. Leite, S. Liu, Y.-L. Loo, J. M. Luther, C.-Q. Ma, M. Madsen, M. Manceau, M. Matheron, M. McGehee, R. Meitzner, M. K. Nazeeruddin, A. F. Nogueira, c. Odabaşı, A. Osherov, N.-G. Park, M. O. Reese, F. De Rossi, M. Saliba, U. S. Schubert, H. J. Snaith, S. D. Stranks, W. Tress, P. A. Troshin, V. Turkovic, S. Veenstra, I. Visoly-Fisher, A. Walsh, T. Watson, H. Xie, R. Yıldırım, S. M. Zakeeruddin, K. Zhu and M. Lira-Cantu, *Nat. Energy*, 2020, **5**, 35–49.

3 Q. Jiang, R. Tirawat, R. A. Kerner, E. A. Gaulding, Y. Xian, X. Wang, J. M. Newkirk, Y. Yan, J. J. Berry and K. Zhu, *Nature*, 2023, 1–2.

4 S. N. Habisreutinger, N. K. Noel and H. J. Snaith, *ACS Energy Lett.*, 2018, **3**, 2472–2476.

5 R. A. Kerner, L. Zhao, S. P. Harvey, J. J. Berry, J. Schwartz and B. P. Rand, *ACS Energy Lett.*, 2020, **5**, 3352–3356.

6 Z. Xu, R. A. Kerner, J. J. Berry and B. P. Rand, *Adv. Funct. Mater.*, 2022, **32**, 2203432.

7 K. Domanski, E. A. Alharbi, A. Hagfeldt, M. Grätzel and W. Tress, *Nat. Energy*, 2018, **3**, 61–67.

8 A. Farooq, M. R. Khan, T. Abzieher, A. Voigt, D. C. Lupascu, U. Lemmer, B. S. Richards and U. W. Paetzold, *ACS Appl. Energy Mater.*, 2021, **4**, 3083–3092.

9 T. Wu, L. K. Ono, R. Yoshioka, C. Ding, C. Zhang, S. Mariotti, J. Zhang, K. Mitrofanov, X. Liu, H. Segawa, R. Kabe, L. Han and Y. Qi, *Energy Environ. Sci.*, 2022, **15**, 4612–4624.

10 Y. Gao, F. Ren, D. Sun, S. Li, G. Zheng, J. Wang, H. Raza, R. Chen, H. Wang, S. Liu, P. Yu, X. Meng, J. He, J. Zhou, X. Hu, Z. Zhang, L. Qiu, W. Chen and Z. Liu, *Energy Environ. Sci.*, 2023, **16**, 2295–2303.

11 Q. Feng, X. Huang, Z. Tang, Y. Hou, Q. Chang, S. Nie, F. Cao, X. Niu, J. Yin, J. Li, N. Zheng and B. Wu, *Energy Environ. Sci.*, 2022, **15**, 4404–4413.

12 T. Wu, X. Xu, L. K. Ono, T. Guo, S. Mariotti, C. Ding, S. Yuan, C. Zhang, J. Zhang, K. Mitrofanov, Q. Zhang, S. Raj, X. Liu, H. Segawa, P. Ji, T. Li, R. Kabe, L. Han, A. Narita and Y. Qi, *Adv. Mater.*, 2023, **35**, 2300169.

13 T. Liu, X. Zhao, P. Wang, Q. C. Burlingame, J. Hu, K. Roh, Z. Xu, B. P. Rand, M. Chen and Y.-L. Loo, *Adv. Energy Mater.*, 2022, 2200402.

14 D. P. McMeekin, P. Holzhey, S. O. Fürer, S. P. Harvey, L. T. Schelhas, J. M. Ball, S. Mahesh, S. Seo, N. Hawkins, J. Lu, M. B. Johnston, J. J. Berry, U. Bach and H. J. Snaith, *Nat. Mater.*, 2023, **22**, 73–83.

15 D. A. Noori, A. Behjat and M. Dehghanipour, *J. Mater. Sci.: Mater. Electron.*, 2023, **34**, 592.

16 C. Ma, M.-C. Kang, S.-H. Lee, S. J. Kwon, H.-W. Cha, C.-W. Yang and N.-G. Park, *Joule*, 2022, **6**, 2626–2643.

17 R. Chen, S. Liu, X. Xu, F. Ren, J. Zhou, X. Tian, Z. Yang, X. Guanz, Z. Liu, S. Zhang, Y. Zhang, Y. Wu, L. Han, Y. Qi and W. Chen, *Energy Environ. Sci.*, 2022, **15**, 2567–2580.

18 J. Sanchez-Diaz, R. S. Sánchez, S. Masi, M. Krečmarová, A. O. Alvarez, E. M. Barea, J. Rodriguez-Romero, V. S. Chirvony, J. F. Sánchez-Royo, J. P. Martinez-Pastor and I. Mora-Seró, *Joule*, 2022, **6**, 861–883.

19 H. Zhu, S. Teale, M. N. Lintangpradipto, S. Mahesh, B. Chen, M. D. McGehee, E. H. Sargent and O. M. Bakr, *Nat. Rev. Mater.*, 2023, **8**, 569–586.

20 A. E. Louks, R. Tirawat, M. Yang, S. N. Habisreutinger, S. P. Harvey, K. Schutt, K. Zhu, J. J. Berry and A. F. Palmstrom, *Sol. RRL*, 2023, **7**, 2300248.

21 S. P. Dunfield, A. E. Louks, J. Waxse, R. Tirawat, S. Robbins, J. J. Berry and M. O. Reese, *Sustainable Energy Fuels*, 2023, **7**, 3294–3305.

22 W. Nie, J.-C. Blancon, A. J. Neukirch, K. Appavoo, H. Tsai, M. Chhowalla, M. A. Alam, M. Y. Sfeir, C. Katan, J. Even, S. Tretiak, J. J. Crochet, G. Gupta and A. D. Mohite, *Nat. Commun.*, 2016, **7**, 11574.

23 T. Duong, H. K. Mulmudi, Y. Wu, X. Fu, H. Shen, J. Peng, N. Wu, H. T. Nguyen, D. Macdonald, M. Lockrey, T. P. White, K. Weber and K. Catchpole, *ACS Appl. Mater. Interfaces*, 2017, **9**, 26859–26866.

24 P. Holzhey, P. Yadav, S.-H. Turren-Cruz, A. Ummadisingu, M. Grätzel, A. Hagfeldt and M. Saliba, *Mater. Today*, 2019, **29**, 10–19.

25 K. Jeong, J. Byeon, J. Jang, N. Ahn and M. Choi, *Joule*, 2022, **6**, 1087–1102.

26 R. A. Kerner, P. Schulz, J. A. Christians, S. P. Dunfield, B. Dou, L. Zhao, G. Teeter, J. J. Berry and B. P. Rand, *APL Mater.*, 2019, **7**, 041103.

27 L. A. Frolova, N. N. Dremova and P. A. Troshin, *Chem. Commun.*, 2015, **51**, 14917–14920.

28 D. A. Jacobs, C. M. Wolff, X.-Y. Chin, K. Artuk, C. Ballif and Q. Jeangros, *Energy Environ. Sci.*, 2022, **15**, 5324–5339.

29 J. Barbé, V. Kumar, M. J. Newman, H. K. H. Lee, S. M. Jain, H. Chen, C. Charbonneau, C. Rodenburg and W. C. Tsoi, *Sustainable Energy Fuels*, 2018, **2**, 905–914.

30 C. Besleaga, L. E. Abramiuc, V. Stancu, A. G. Tomulescu, M. Sima, L. Trinca, N. Plugaru, L. Pintilie, G. A. Nemnes, M. Iliescu, H. G. Svavarsson, A. Manolescu and I. Pintilie, *J. Phys. Chem. Lett.*, 2016, **7**, 5168–5175.

31 C. Ding, L. Yin, L. Zhang, R. Huang, S. Fan, Q. Luo, J. Lin, F. Li, C. Zhao, R. Österbacka and C.-Q. Ma, *Adv. Funct. Mater.*, 2021, **31**, 2103820.

32 Y. Kato, L. K. Ono, M. V. Lee, S. Wang, S. R. Raga and Y. Qi, *Adv. Mater. Interfaces*, 2015, **2**, 1500195.

33 C. C. Boyd, R. Cheacharoen, K. A. Bush, R. Prasanna, T. Leijtens and M. D. McGehee, *ACS Energy Lett.*, 2018, **3**, 1772–1778.

34 K. Xiao, Y.-H. Lin, M. Zhang, R. D. J. Oliver, X. Wang, Z. Liu, X. Luo, J. Li, D. Lai, H. Luo, R. Lin, J. Xu, Y. Hou, H. J. Snaith and H. Tan, *Science*, 2022, **376**, 762–767.